A General Simplification and Acceleration Method for Distribution System Optimization Problems

Jun Xiao, *Member*, *IEEE*, Yupeng Zhou, *Student Member*, *IEEE*, Buxin She, *Member*, *IEEE*, and Zhenyu Bao

***Abstract*—Solving optimization problems plays a vital role in ensuring the secure and economic operation of distribution systems. To enhance computational efficiency, this paper proposes a general simplification and acceleration method for distribution system optimization problems. Firstly, the capacity boundary and voltage boundary model of distribution systems are established. The relative position between the two boundaries reflects the strength of capacity and voltage constraints, leading to the definition of two critical feeder lengths (CFLs) to quantify these strengths. Secondly, simplification criteria and an acceleration method are proposed. Given a distribution system, if the distance from the end load/DG node to the slack bus is less than the corresponding CFL, we can conclude that the capacity constraints are stricter than the voltage constraints. Then, the distribution system can be simplified by adopting DC power flow model or disregarding the voltage constraints. After that, the reference value tables of CFL are presented. Finally, the effectiveness of the proposed method is verified by exemplifying the method in network reconfiguration and reactive power optimization problems. By implementing the proposed acceleration method, a significant reduction in computation time is achieved while ensuring accuracy. This method applies to most urban distribution systems in optimization problems involving power flow equations or voltage constraints.**

***Index Terms*—Distribution system, optimization problem, power flow equation, security region, simplification criteria, acceleration method, network reconfiguration, reactive power optimization.**

Received: March 2, 2024
Accepted: August 27, 2024
Published Online: January 1, 2025

Jun Xiao and Yupeng Zhou are with the Key Laboratory of the Ministry of Education on Smart Power Grids, Tianjin University, Tianjin 300072, China (e-mail: xiaojun@ tju.edu.cn; yupengzhou2000@163.com).

Buxin She (correspondence author) is with the Department of Electrical Engineering & Computer Science, University of Tennessee Knoxville, TN 37996, USA (e-mail: bshe@vols.utk.edu).

Zhenyu Bao is with the Ningbo Power Supply Company of State Grid Zhejiang Electric Power Co., Ltd., Ningbo 315000, China (e-mail: baozhenyu@tju.edu.cn).

DOI:10.23919/PCMP.2023.000210

NOMENCLATURE

A. Abbreviations

CFL	critical feeder length
DG	distributed generation
TSC	total supply capability
DSSR	distribution system security region
PF	power factor
VRM	voltage regulation measure
OLTC	on-load tap changer
RPC	reactive power compensation
RPA	reactive power absorption

B. Variables

f	the weighted summation's objective function
$P(i)_{\text{cut}}$	the active power of outage load node i after restoration
$P(i_0)_{\text{cut}}$	the active power of outage load node i_0 before restoration
$L(j)_{\text{cut}}$	the load coefficient of the outage load node j after restoration
$L(j_0)_{\text{cut}}$	the load coefficient of the outage load node j_0 before restoration
$K(k)$	the action state of the kth switch
M	the total number of outage load nodes after restoration
M_0	the total number of outage load nodes before restoration
N	the total number of switches
a, b, c	weight coefficient of objective function
g_k	the post-fault network reconfiguration
G_R	the set of all possible radial reconfigurations
F	the augmented objective function
P_{loss}	active power loss of distribution system
m	number of distribution system branches
G_{ij}	the conductance between node i and node j
B_{ij}	the susceptance between node i and node j

λ	penalty factor of penalty function
ΔU_i	voltage magnitude deviation of node i
U_i	voltage magnitude of node i
U_j	voltage magnitude of node j
$U_{i,\min}$	the minimum value of the voltage magnitude of node i
$U_{i,\max}$	the maximum value of the voltage magnitude of node i
θ_i	the voltage phase angle node i
θ_j	the voltage phase angle node j
θ_{ij}	the voltage phase angle difference between node i and node j
P_i	active power of node i
Q_i	reactive power of node i
$Q_{\mathrm{DG},x}$	the xth distributed generation reactive power output
$Q_{\mathrm{DG},x,\min}$	the minimum value of the xth distributed generation reactive power output
$Q_{\mathrm{DG},x,\max}$	the maximum value of the xth distributed generation reactive power output
$Q_{\mathrm{C},y}$	capacity of the yth reactive power compensation device
$Q_{\mathrm{C},y,\min}$	the minimum value of capacity of the yth reactive power compensation device
$Q_{\mathrm{C},y,\max}$	the maximum value of capacity of the yth reactive power compensation device
S_{ij}	the branch capacity between node i and node j
$S_{ij,\max}$	the maximum value of the branch capacity between node i and node j

C. Symbols

$\boldsymbol{\Omega}_{\mathrm{AC}}$	security region of AC power flow model
$\boldsymbol{\Omega}_{\mathrm{TQSR0,AC}}$	total quadrants security region
$\partial\boldsymbol{\Omega}^{+}_{\mathrm{s-I}}$	forward capacity boundary
$\partial\boldsymbol{\Omega}^{-}_{\mathrm{s-I}}$	reverse capacity boundary
$\partial\boldsymbol{\Omega}^{-}_{\mathrm{s-U}}$	lower voltage boundary
$\partial\boldsymbol{\Omega}^{+}_{\mathrm{s-U}}$	upper voltage boundary
$L_{\mathrm{c,L}}$	critical feeder length for load
$L_{\mathrm{c,DG}}$	critical feeder length for DG
$\boldsymbol{W}$	operation point vector
$\boldsymbol{\Theta}$	state space
$\boldsymbol{\Theta}_{\mathrm{ADN}}$	state space of active distribution network
$\boldsymbol{\Theta}^{+}_{\mathrm{I}}$	forward capacity region
$\boldsymbol{\Theta}^{-}_{\mathrm{I}}$	reverse capacity region
$\boldsymbol{\Theta}^{-}_{\mathrm{U}}$	lower voltage region
$\boldsymbol{\Theta}^{+}_{\mathrm{U}}$	upper voltage region
$\boldsymbol{E}$	Euclidean space
$g_{N-0}(\boldsymbol{W})\leqslant 0$	N-0 security constraints
$B(\boldsymbol{W};r)$	the set of all operating points in a sphere with operating points $\boldsymbol{W}$ as the center of the sphere and r as the radius

I. Introduction

The smart grid represents a prominent focal point of current research [1], with the distribution system being a crucial element. To advance the utilization of renewable energy sources and work towards achieving "zero carbon" emissions, it is essential to improve the control and optimization of the distribution system. This is particularly crucial given the rising uncertainties associated with these systems. The optimization problem related to the operation of the distribution system strives to achieve a secure, cost-effective, and efficient operational state by adjusting control variables to meet operational constraints [2].

Power flow calculation serves as the fundamental tool in distribution system analysis and finds extensive application in the control and optimization of distribution systems. Examples of its utilization include determining the locational marginal price [3], [4], coordinating the EV charging problem [5], optimizing reactive power [6], reconfiguring networks [7], assessing the maximum output of distributed generations (DGs) [8], and calculating the total supply capability (TSC) [9]. The standard AC power flow analysis of a distribution system involves solving a set of nonlinear algebraic equations [10]. Common methods for solving these equations encompass the Newton method [11], backward/forward sweep power flow technique [12], implicit Z_{bus} Gauss method [13], and loop-analysis method [14].

Whereas the AC power flow model can accurately depict the power flow within a distribution system, they transform the optimization problem into a nonlinear and intricate challenge. This complexity can impede convergence and introduce inefficiencies into the solving process, making it challenging to apply these methods to large-scale distribution systems [15]. The efficiency of the solution plays a pivotal role in determining the practical implementation of the model algorithm for online distribution system optimization. To enhance computational efficiency, it is a common practice to simplify the power flow equation or power flow constraints. Existing research typically employs two simplified approaches: one involves convex relaxation of the nonlinear AC equality constraints into inequality constraints, and the other entails transforming the nonlinear AC power flow equations into linear power flow equations [16].

The successful implementation of the convex relaxation method hinges on ensuring that both the objective

function and boundary conditions strictly adhere to the relaxation conditions; otherwise, substantial solution errors may arise [16]. In [17] and [18], a two-step convex relaxation method is introduced for the branch flow model. This method combines phase angle relaxation and conic relaxation, and its accuracy is substantiated. In [19], the dynamic network reconfiguration model is transformed into a mixed-integer second-order cone programming problem through the utilization of the second-order cone relaxation method. This transformation effectively reduces the computational complexity of solving the model. However, the convex relaxation method encounters challenges related to high computational demands and relaxation accuracy, which have limited its widespread adoption in industrial applications.

In contrast, the method of linearizing the AC power flow equation is widely used. DC power flow model stands out as the most classical linear power flow model [20]. For example, in [8], the DC power flow model is applied to streamline the assessment of the maximum DG output in active distribution networks, leading to a significant enhancement in assessment speed. In [9], it is found that urban distribution systems typically feature relatively short feeder lengths, thus the use of the DC power flow model for simplification is acceptable. Although this model is friendly for computation, it does entail a sacrifice in accuracy. Apart from the DC power flow model, many research have proposed various linearization methods. For example, in terms of power flow solution, [15] proposes an approximate linear power flow model by employing a logarithmic transformation of voltage magnitude, which exhibited greater accuracy compared to existing linear power flow models. In [21], a linearized power flow model is proposed, considering voltage magnitude but omitting the distribution of reactive power.

In the context of distribution system optimization, several methods have been introduced. Reference [3] linearizes the voltage magnitude and phase angle, and omitted the 2nd and higher order terms of the Taylor series related to active and reactive power loss, thus reducing computational burden while preserving the accuracy of locational marginal price calculations. Reference [4] introduces a power flow linearization technique employing 2nd-order Taylor series expansions of sine and cosine functions related to power distribution and the loss factor method, thereby enhancing the accuracy of locational marginal price calculations. In [5], the nonlinear terms of the branch power flow equations are ignored in EV charging problem, and the calculation speed is faster than the existing method without compromising accuracy. In [3]–[5], [15], and [21], a fundamental assumption is made, requiring that voltage phase angle difference between nodes is exceedingly small and voltage magnitude of each node is roughly equivalent. However, it is crucial to recognize that this assumption does come with certain limitations when applied in practical scenarios.

Current research primarily emphasizes the linearization and simplification of the power flow model tailored to specific optimization problems. However, there remain few investigations into a generalized simplification method for the power flow model that can be applied to various optimization problems. In [16] within the domain of reactive power optimization and network reconfiguration, a novel approach is adopted wherein the ratio of active power and reactive power to voltage magnitude is considered as new state variables. However, the comprehensive optimization model for reactive power optimization and network reconfiguration still constitutes a singular optimization problem.

This paper conducts a comprehensive overview of existing references [3]–[5], [8], [9], [15], [16], [21] pertaining to research methods for simplifying power flow models in distribution system optimization problems. They primarily focus on the simplification of power flow models, attributing to the relatively short lengths of distribution lines and the prevalent usage of cable lines. Additionally, it is observed that in such cases, voltage drops, and network losses are typically small. The existing studies rely on qualitative methods to determine the feasibility of simplification and often lack quantitative criteria. Hence, this paper bridges the gap by proposing a general simplification criteria and acceleration method for distribution system optimization problems integrating power flow equations or voltage constraints.

The recent development on the distribution system security region (DSSR) [27] theory provides a new perspective to simplify the distribution system optimization problems with power flow equations or voltage constraints. Reference [22] finds the relative strictness between the voltage constraints and the capacity constraints. The DSSR security boundary is divided into capacity boundary and voltage boundary. When visualizing a DSSR, the relative position between capacity boundary and voltage boundary shows the strictness of corresponding constraints [22]. Reference [22] proposes a method to judge whether DC power flow model can be used; however, it is not applicable to active distribution networks. Reference [23] further extends the method of [22] to the active distribution network. However, the method in [23] is not applicable in scenarios requiring the calculation of voltage or network loss, as it uniformly simplifies to a DC power flow model, incapable of providing voltage and network loss information. What's more, the method of [23] is only used for the power flow model selection of one optimization problem, and a general simplification and acceleration method has not yet been formed.

Inspired by [22], [23], this paper proposes a general simplification and acceleration method for distribution system optimization problems integrating power flow equations or voltage constraints based on DSSR. This paper unveils a significant finding within real power grids, especially urban power grids, where a substantial portion of distribution systems align with the established simplification criteria. As long as the optimization problem involves power flow equations or voltage constraints, they can be simplified and accelerated. Then, the contributions of this paper are as follows:

1) Formulation of a set of precise simplification cri-

teria. By examining the relationship between the distance from the end load/DG node to the slack bus and the corresponding CFL, these criteria serve as tools for assessing the feasibility of simplification.

2) Development of an efficient acceleration method. For a distribution system that meets the simplification criteria, the optimization problems entailing power flow equations or voltage constraints can be seamlessly integrated into the acceleration method.

3) Demonstrating the adaptability and acceleration efficacy of the proposed method in a variety of classical optimization problems.

The rest of this paper is organized as follows. The capacity boundary and voltage boundary model of DSSR are established in Section II. Then, Section III introduces the simplification criteria and acceleration method. Section IV calculates CFL and forms the reference value tables of CFL. Sections V and VI verify the proposed method in network reconfiguration and reactive power optimization problems, respectively. Section VII encapsulates the conclusions and offers insights into future work. For reference, a comprehensive list of key terminology can be found in Appendix A.

II. Security Boundary of Distribution System

This section introduces the preliminary definition of security boundary of distribution system, including the operation point, state space, AC power flow model, security boundary, capacity boundary, and voltage boundary.

A. Operating Point and State Space

1) Operating Point of DSSR

For a distribution system with n load/DG nodes, the operating point $\boldsymbol{W}$ for security analysis is expressed as follows [22]:

$$\boldsymbol{W}=\left[\dot{S}_1,\dot{S}_2,\cdots,\dot{S}_i,\cdots,\dot{S}_n\right]^{\mathrm{T}} \tag{1}$$

$$\dot{S}_i=\begin{cases}\dot{S}_{\mathrm{L},i}, i\in\boldsymbol{L}\\ \dot{S}_{\mathrm{DG},i}, i\in\boldsymbol{G}\end{cases} \tag{2}$$

where $\dot{S}_i=P_i+\mathrm{j}Q_i$ is the net complex power of node i; $\boldsymbol{L}$ is the set of load nodes; and $\boldsymbol{G}$ is the set of DG nodes. For a load node i, the corresponding complex power is denoted as $\dot{S}_{\mathrm{L},i}$, and for a DG node, the corresponding complex power is denoted as $\dot{S}_{\mathrm{DG},i}$.

2) State Space of DSSR

In real operation, the node power undergoes variations within a certain range, and operating points that exceed the maximum allowable range are not taken into consideration in [24]. Assuming positive power outflow from nodes, the state space $\boldsymbol{\Theta}_{\mathrm{ADN}}$ of the distribution system is defined as:

$$\boldsymbol{\Theta}_{\mathrm{ADN}}=\left\{\boldsymbol{W}\left|\begin{matrix}0\leqslant\left|\dot{S}_{\mathrm{L},i}\right|\leqslant\left|\dot{S}_{\mathrm{L},i,\max}\right|\\ 0\leqslant\left|\dot{S}_{\mathrm{DG},i}\right|\leqslant\left|\dot{S}_{\mathrm{DG},i,\max}\right|\end{matrix}\right.\right\} \tag{3}$$

where $\left|\dot{S}_{\mathrm{L},i,\max}\right|$ is the maximum power of load node i and $\left|\dot{S}_{\mathrm{DG},i,\max}\right|$ is the maximum power of DG node i.

B. Model of DSSR

Under normal operating conditions, the AC power flow model of the DSSR [25] is represented by (4).

$$\boldsymbol{\Omega}_{\mathrm{TQSR0,AC}}=\left\{\boldsymbol{W}\in\boldsymbol{\Theta}\left|f(U,\theta)=\boldsymbol{W},g_{N-0}(\boldsymbol{W})\leqslant 0\right.\right\} \tag{4}$$

where $f(U,\theta)=\boldsymbol{W}$ is the power flow equation; and $g_{N-0}(\boldsymbol{W})\leqslant 0$ are the N–0 security constraints. The N–0 security constraints encompass the branch capacity constraints (5) and the node voltage constraints (6).

$$\left|\sum_{j\in\boldsymbol{\Omega}_{\mathrm{B},i}}\dot{S}_j+\dot{S}_{\mathrm{loss},i}\right|\leqslant c_{\mathrm{B},m}(\forall i\in m) \tag{5}$$

where $\boldsymbol{\Omega}_{\mathrm{B},i}$ is the set of all nodes between the node i and the end node of feeder; $\dot{S}_{\mathrm{loss},i}$ is the power loss of all branches between the node i and the end node of feeder under normal system operation; $c_{\mathrm{B},m}$ is the capacity of the feeder m; and $i\in m$ indicates that the node i belongs to feeder m.

$\mathrm{Re}\left(\sum_{j\in\boldsymbol{\Omega}_{\mathrm{B},i}}\dot{S}_j+\dot{S}_{\mathrm{loss},i}\right)>0$ indicates the forward power flow, and the corresponding capacity constraints are referred to as forward capacity constraints; $\mathrm{Re}\left(\sum_{j\in\boldsymbol{\Omega}_{\mathrm{B},i}}\dot{S}_j+\dot{S}_{\mathrm{loss},i}\right)<0$ indicates the reverse power flow, and the corresponding capacity constraints are known as reverse capacity constraints.

$$U_{i,\min}\leqslant U_i\leqslant U_{i,\max} \tag{6}$$

where $U_{i,\max}$ is the upper voltage limit of node i; and $U_{i,\min}$ is the lower voltage limit of node i.

C. Security Boundary of DSSR

The security boundary of a distribution system comprises operating points that exhibit critical security, which means each point on this boundary is associated with a minimum load increase that would render the system insecure [26]. The determination of the security boundary for the distribution system is reliant on various parameters, including the topology of the distribution system, component capacities, and operational measures such as voltage regulation [27].

In the case of traditional distribution networks, the security boundary is divided into capacity boundary and voltage boundary in [22] to analyze the impact of voltage constraints and capacity constraints on the security boundary. Considering the characteristics of active distribution networks, building upon the work presented in [22], the capacity boundary is further classified into forward capacity boundary and reverse capacity boundary, whereas the voltage boundary is

divided into upper voltage boundary and lower voltage boundary.

D. Capacity Region and Capacity Boundary

1) Capacity Region

Capacity region is the set of all operating points in the state space that satisfy the capacity constraints.

a) Forward Capacity Region

Forward capacity region is the set of all operating points in the state space that satisfy the forward capacity constraints as defined in (5) and is denoted as $\boldsymbol{\Theta}_{\mathrm{I}}^{+}$. The mathematical model for $\boldsymbol{\Theta}_{\mathrm{I}}^{+}$ is shown in (7).

$$\boldsymbol{\Theta}_{\mathrm{I}}^{+}=\left\{\boldsymbol{W}\left|\begin{array}{l}\left|\sum_{j\in\boldsymbol{\Omega}_{\mathrm{B},i}}\dot{S}_j+\dot{S}_{\mathrm{loss},i}\right|\leqslant c_{\mathrm{B},m}(\forall i\in m)\\ \mathrm{Re}(\sum_{j\in\boldsymbol{\Omega}_{\mathrm{B},i}}\dot{S}_j+\dot{S}_{\mathrm{loss},i})>0\end{array}\right.\right\} \tag{7}$$

b) Reverse Capacity Region

Reverse capacity region is the set of all operating points in the state space that satisfy the reverse capacity constraints as defined in (5) and is denoted as $\boldsymbol{\Theta}_{\mathrm{I}}^{-}$. The mathematical model for $\boldsymbol{\Theta}_{\mathrm{I}}^{-}$ is shown in (8).

$$\boldsymbol{\Theta}_{\mathrm{I}}^{-}=\left\{\boldsymbol{W}\left|\begin{array}{l}\left|\sum_{j\in\boldsymbol{\Omega}_{\mathrm{B},i}}\dot{S}_j+\dot{S}_{\mathrm{loss},i}\right|\leqslant c_{\mathrm{B},m}(\forall i\in m)\\ \mathrm{Re}(\sum_{j\in\boldsymbol{\Omega}_{\mathrm{B},i}}\dot{S}_j+\dot{S}_{\mathrm{loss},i})<0\end{array}\right.\right\} \tag{8}$$

2) Capacity Boundary

The security boundary in distribution system is influenced by both branch capacity constraints and node voltage constraints. When the voltage constraints are ignored, the security boundary is determined solely by the capacity constraints, referred to as the capacity boundary [22]. In active distribution networks, the capacity boundary is further divided into the forward capacity boundary and the reverse capacity boundary.

a) Forward Capacity Boundary

When the power flow reaches the forward boundary, an increase in load or a decrease in DG output typically results in a violation of the forward capacity constraints. In such cases, the capacity boundary corresponds to the forward capacity boundary and is denoted as $\partial\boldsymbol{\Omega}_{\mathrm{s-I}}^{+}$. The mathematical model for $\partial\boldsymbol{\Omega}_{\mathrm{s-I}}^{+}$ is shown in (9).

$$\partial\boldsymbol{\Omega}_{\mathrm{s-I}}^{+}=\left\{\boldsymbol{W}\left|\begin{array}{l}\forall r>0,\\ B(\boldsymbol{W};r)\bigcap\boldsymbol{\Theta}_{\mathrm{I}}^{+}\neq\varnothing\\ B(\boldsymbol{W};r)\bigcap(\boldsymbol{\Theta}-\boldsymbol{\Theta}_{\mathrm{I}}^{+})\neq\varnothing\end{array}\right.\right\} \tag{9}$$

where $B(\boldsymbol{W};r)$ is the set of all operating points in a sphere with operating points $\boldsymbol{W}$ as the center of the sphere and r as the radius.

b) Reverse Capacity Boundary

When the power flow reaches the reverse boundary, a decrease in load or an increase in DG output typically results in a violation of the reverse capacity constraints. In such cases, the capacity boundary corresponds to the reverse capacity boundary and is denoted as $\partial\boldsymbol{\Omega}_{\mathrm{s-I}}^{-}$. The mathematical model for $\partial\boldsymbol{\Omega}_{\mathrm{s-I}}^{-}$ is shown in (10).

$$\partial\boldsymbol{\Omega}_{\mathrm{s-I}}^{-}=\left\{\boldsymbol{W}\left|\begin{array}{l}\forall r>0,\\ B(\boldsymbol{W};r)\bigcap\boldsymbol{\Theta}_{\mathrm{I}}^{-}\neq\varnothing\\ B(\boldsymbol{W};r)\bigcap(\boldsymbol{\Theta}-\boldsymbol{\Theta}_{\mathrm{I}}^{-})\neq\varnothing\end{array}\right.\right\} \tag{10}$$

E. Voltage Region and Voltage Boundary

1) Voltage Region

Voltage region is the set of all operating points in the state space that satisfy the voltage constraints.

a) Lower Voltage Region

Lower voltage region is the set of all operating points in the state space that satisfy the lower voltage constraints as defined in (6) and is denoted as $\boldsymbol{\Theta}_{\mathrm{U}}^{-}$. The mathematical model for $\boldsymbol{\Theta}_{\mathrm{U}}^{-}$ is shown in (11).

$$\boldsymbol{\Theta}_{\mathrm{U}}^{-}=\left\{\boldsymbol{W}\left|U_{i,\min}\leqslant U_i(\forall i)\right.\right\} \tag{11}$$

b) Upper Voltage Region

Upper voltage region is the set of all operating points in the state space that satisfy the upper voltage constraints as defined in (6) and is denoted as $\boldsymbol{\Theta}_{\mathrm{U}}^{+}$. The mathematical model for $\boldsymbol{\Theta}_{\mathrm{U}}^{+}$ is shown in (12).

$$\boldsymbol{\Theta}_{\mathrm{U}}^{+}=\left\{\boldsymbol{W}\left|U_i\leqslant U_{i,\max}(\forall i)\right.\right\} \tag{12}$$

2) Voltage Boundary

When the capacity constraints are ignored, the security boundary is solely determined by the voltage constraints, known as the voltage boundary [22]. In active distribution networks, the voltage boundary is further divided into the lower voltage boundary and the upper voltage boundary.

a) Lower Voltage Boundary

When the voltage magnitude reaches the lower voltage boundary, an increase in load or a decrease in DG output typically results in a violation of the lower voltage constraints. In such cases, the voltage boundary corresponds to the lower voltage boundary and is denoted as $\partial\boldsymbol{\Omega}_{\mathrm{s-U}}^{-}$. The mathematical model for $\partial\boldsymbol{\Omega}_{\mathrm{s-U}}^{-}$ is presented in (13).

$$\partial\boldsymbol{\Omega}_{\mathrm{s-U}}^{-}=\left\{\boldsymbol{W}\left|\begin{array}{l}\forall r>0,\\ B(\boldsymbol{W};r)\bigcap\boldsymbol{\Theta}_{\mathrm{U}}^{-}\neq\varnothing\\ B(\boldsymbol{W};r)\bigcap(\boldsymbol{\Theta}-\boldsymbol{\Theta}_{\mathrm{U}}^{-})\neq\varnothing\end{array}\right.\right\} \tag{13}$$

b) Upper Voltage Boundary

When the voltage magnitude reaches the upper voltage boundary, a decrease in load or an increase in DG output typically results in a violation of the upper voltage constraints. In such cases, the voltage boundary

corresponds to the upper voltage boundary and is denoted as $\partial\boldsymbol{\Omega}^{+}_{\mathrm{s-U}}$. The mathematical model for $\partial\boldsymbol{\Omega}^{+}_{\mathrm{s-U}}$ is presented in (14).

$$\partial\boldsymbol{\Omega}^{+}_{\mathrm{s-U}}=\left\{\boldsymbol{W}\left|\begin{array}{l}\forall r>0,\\ B(\boldsymbol{W};r)\bigcap\boldsymbol{\Theta}^{+}_{\mathrm{U}}\neq\varnothing\\ B(\boldsymbol{W};r)\bigcap(\boldsymbol{\Theta}-\boldsymbol{\Theta}^{+}_{\mathrm{U}})\neq\varnothing\end{array}\right.\right\} \tag{14}$$

III. Simplification and Acceleration Method

The application of the proposed method is divided into two phases. Phase 1: establishment of reference value tables of CFL; Phase 2: simplification and acceleration. In Phase 2, different optimization problems can be calculated multiple times without the need to recompute CFL each time. Then, the lookup of the table is sufficient. A single computation of CFL is required only when a specific CFL value is not found in the tables. The calculated value can be added to the reference value tables for further usage. The following sections detail the methods for these two phases, concluding with a discussion on the applicable subjects and scenarios.

A. Critical Feeder Length

1) Concept of Critical Feeder Length

The acceleration method is based on analyzing the interplay between the strength of capacity constraints and voltage constraints in relation to the power supply length of the feeder. In the AC power flow of a distribution system, both forward and reverse capacity constraints, as well as upper and lower voltage constraints, are considered. Recent studies on the security boundary of distribution system have indicated that the strength relationship between capacity constraints and voltage constraints can be easily determined by the relative position of the capacity boundary and voltage boundary.

This study observes that the strength relationship between these constraints is closely linked to the distance from the end load or DG node to the slack bus. Consequently, CFLs for load and DG are defined separately. If the distance from the end load/DG node of the distribution system to the slack bus is less than the corresponding CFL, the system can be simplified and accelerated by adopting the DC power flow model or by disregarding the voltage constraints. This method enables more efficient and practical analyses by considering the specific characteristics of the distribution system.

2) Definition of Critical Feeder Length

When DGs are integrated into the distribution system, it introduces both power outflows and inflows at various nodes, leading to a transformation of power flow direction from uni-directional to bi-directional. The distribution of load and DG in the main trunk of the active distribution network is depicted in Fig. 1, where $\dot{S}_{\mathrm{loss},m}$ is the network loss on branch m; U_{S} is the voltage magnitude of the slack bus; $P_n+\mathrm{j}Q_n$ is the accessed equivalent load.

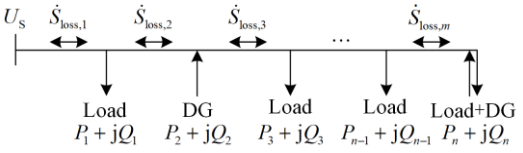

Fig. 1. Feeder model of active distribution network.

The power flow may reach the reverse boundary, and the voltage magnitude may reach the upper voltage boundary in active distribution network. Hence, based on the CFL proposed in reference [22], this paper proposes the definitions of CFL for load and CFL for DG, and accordingly forms the simplification criteria.

When the power flow reaches the forward boundary and the voltage magnitude reaches the lower voltage boundary, it is caused by the load. Therefore, the CFL for load is defined, as shown in **Definition 1**. When the power flow reaches the reverse boundary, and the voltage magnitude reaches the upper voltage boundary, it is caused by the DG. Hence, the CFL for DG is defined, as shown in **Definition 2**.

Definition 1: Critical Feeder Length for Load

It is defined as the critical length of the distance from the end load node to the slack bus in the distribution system, symbolized as $L_{\mathrm{c,L}}$. The mathematical model of CFL for load is presented in (15).

$$\begin{cases}\boldsymbol{\Theta}^{+}_{\mathrm{I}}\subset\boldsymbol{\Theta}^{-}_{\mathrm{U}},\ L_{\mathrm{d,L}}<L_{\mathrm{c,L}}\\ \boldsymbol{\Theta}^{-}_{\mathrm{U}}\subset\boldsymbol{\Theta}^{+}_{\mathrm{I}},\ L_{\mathrm{d,L}}>L_{\mathrm{c,L}}\end{cases} \tag{15}$$

where $L_{\mathrm{d,L}}$ is the distance from the end load node to the slack bus.

$L_{\mathrm{c,L}}$ is used to distinguish the strength relationship between the forward capacity constraints and the lower voltage constraints. $L_{\mathrm{d,L}}<L_{\mathrm{c,L}}$ means that the feeder length is relatively short, and the voltage loss is not significant, and the forward capacity constraints are stricter than the lower voltage constraints. This relationship is manifested on the security region such that the forward capacity region $\boldsymbol{\Theta}^{+}_{\mathrm{I}}$ becomes a proper subset of the lower voltage region $\boldsymbol{\Theta}^{-}_{\mathrm{U}}$, thus allowing the lower voltage constraints to be neglected.

Definition 2: Critical Feeder Length for DG

It is defined as the critical length of the distance from the end DG node to the slack bus in the distribution system, symbolized as $L_{\mathrm{c,DG}}$. The mathematical model of CFL for DG is presented in (16).

$$\begin{cases}\boldsymbol{\Theta}^{-}_{\mathrm{I}}\subset\boldsymbol{\Theta}^{+}_{\mathrm{U}},\ L_{\mathrm{d,DG}}<L_{\mathrm{c,DG}}\\ \boldsymbol{\Theta}^{+}_{\mathrm{U}}\subset\boldsymbol{\Theta}^{-}_{\mathrm{I}},\ L_{\mathrm{d,DG}}>L_{\mathrm{c,DG}}\end{cases} \tag{16}$$

where $L_{\mathrm{d,DG}}$ is the distance from the end DG node to the slack bus.

Similarly, when condition $L_{\mathrm{d,DG}} < L_{\mathrm{c,DG}}$ is satisfied, the reverse capacity region $\boldsymbol{\Theta}_{\mathrm{I}}^{-}$ becomes a proper subset of the upper voltage region $\boldsymbol{\Theta}_{\mathrm{U}}^{+}$, thus allowing the upper voltage constraints to be neglected.

3) Calculation of Critical Feeder Length

To calculate CFL, it is simplified based on the feeder model depicted in Fig. 1, resulting in an equivalent feeder model for both forward power flow and reverse power flow, as illustrated in Fig. 2; $R_l + \mathrm{j}X_l$ is the equivalent impedance of the line.

To calculate the CFL based on the feeder model of Fig. 2, the following data are required: 1) Conductor type and its parameters, including unit resistance, unit reactance, and current-carrying capacity; 2) System operation parameters, encompassing power factor (PF) on the load/DG side, voltage regulation measures (VRMs), permissible voltage range at load/DG node. The value of CFL is influenced by the data above, and has nothing to do with the capacity of DG and the level of the load. The reason is that the capacity of DG and the level of the load do not affect the security boundary [27], but the operating point.

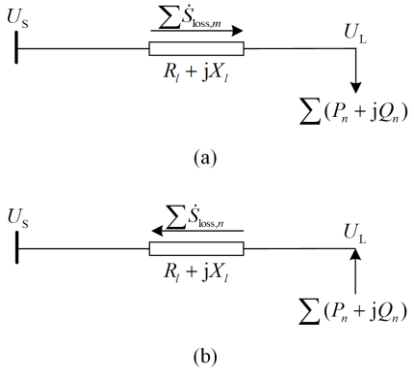

Fig. 2. Simplified feeder model in active distribution network. (a) Equivalent feeder model under forward power flow. (b) Equivalent feeder model under reverse power flow.

Figure 3 shows the flow charts of calculating the CFL for load/DG.

In Fig. 3, C_{pu}^{+} represents the total load per unit value corresponding to the forward capacity boundary point; V_{pu}^{-} represents the total load per unit value corresponding to the lower voltage boundary point; C_{pu}^{-} represents the total DG per unit value corresponding to the reverse capacity boundary point; V_{pu}^{+} represents the total DG per unit value corresponding to the upper voltage boundary point.

Real distribution networks use a finite number of conductor types, which allows for the CFL to be pre-calculated and established into reference value tables of CFL, which constitutes phase 1 of the proposed method. Consequently, this method eliminates the need for recalculating CFL during optimization analysis and simplification of distribution networks in phase 2, as CFL can be directly retrieved from the table, thereby reducing computation time.

By employing the method illustrated in Fig. 3, and altering conductor type and system operation parameters, reference value tables of CFL for load/DG under typical conductors, PF, and VRMs could be formed.

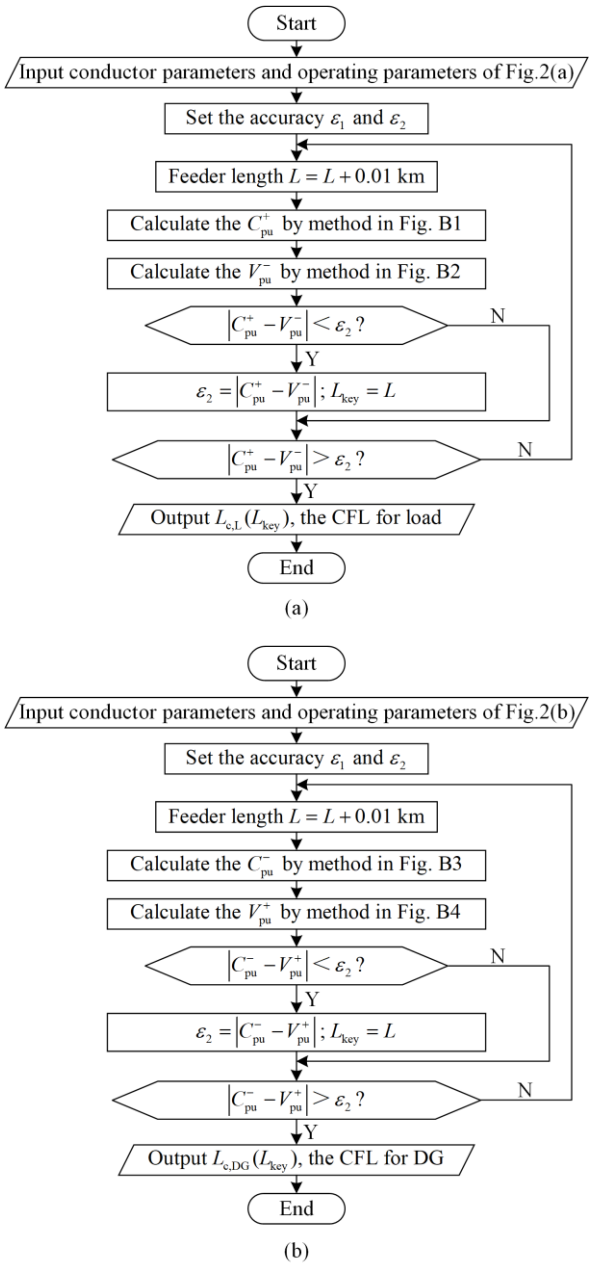

Fig. 3. Calculation methods of critical feeder length for load/DG. (a) Critical feeder length for load. (b) Critical feeder length for DG.

B. Acceleration Method

Once the reference value tables for CFL are established in phase 1, the next step is to proceed to phase 2: simplification and acceleration. The general method for simplifying and accelerating distribution system optimization problems that involve power flow equations or voltage constraints is shown in Fig. 4.

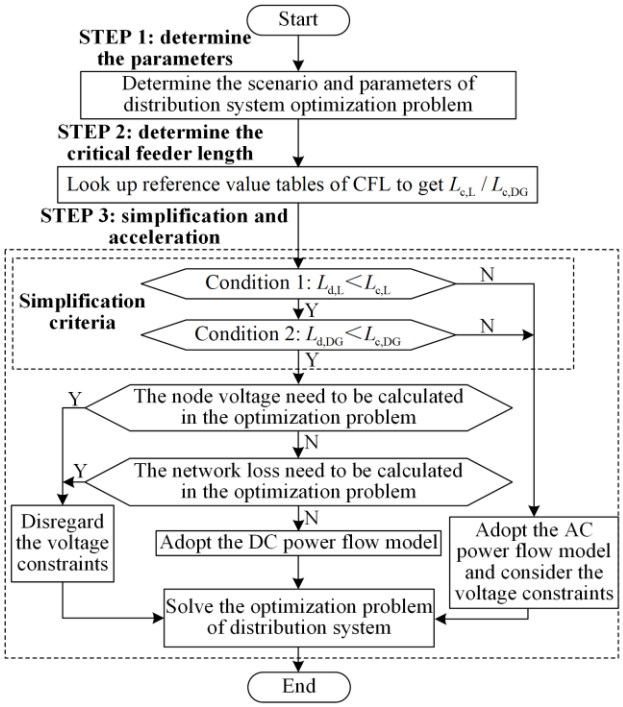

Fig. 4. A general simplification and acceleration process for distribution system optimization problems integrating power flow equations or voltage constraints.

C. Application Guidelines

The proposed method is applicable to the distribution systems with a slack bus. Typically, the slack bus in a distribution system is a 10 kV bus at the substation, providing frequency and voltage support. While this method is suitable for traditional distribution networks, its applicability to active distribution networks requires evaluation on a case-by-case basis.

The proposed method is applicable to an active distribution system connected to a large power grid. However, its applicability may vary when the system is partially islanded. In the case of a single DG in the islanded section, the situation is akin to the normal operation of a traditional distribution network, making the method applicable. Similarly, if multiple DGs are controlled using a master-slave strategy [28], where one DG maintains system voltage and frequency through constant-voltage and constant-frequency control, a slack bus is present, making the method applicable.

However, if the peer-to-peer control [29] or the integrated control strategy [30] is adopted — where multiple grid-forming DGs with droop control manage the system's voltage and frequency without a slack bus-the method is not applicable. For isolated small-scale distribution networks, such as island distribution networks, the applicability of the method depends on the presence of a slack bus. If a slack bus is present, the method is applicable; otherwise, it is not.

As summarized in Fig. 5, the method is applicable to distribution systems with a slack bus, traditional distribution networks, and active distribution networks under specific conditions, as outlined above.

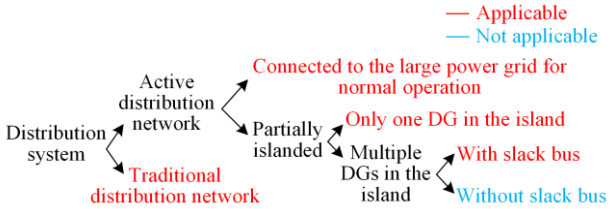

Fig. 5. Summary of applicability of the method.

The proposed method is applicable to a diverse range of scenarios involving optimization problems integrating power flow equations or voltage constraints. This versatility allows for its utilization in various applications, including power flow calculation, reactive power optimization, network reconfiguration, optimal DG allocation, DG maximum output evaluation, marginal price calculation, electric vehicle charging problems, and TSC calculation.

However, it is essential to acknowledge that the simplification and acceleration method may not be universally applicable to all distribution systems. Careful consideration of the specific characteristics and conditions of each distribution system is crucial to employing this method.

IV. Calculation of Critical Feeder Length

A. Calculation Example of CFL

Utilizing the method from Section III-A-3, this section demonstrates how to calculate the CFL for the load of LGJ-185 distribution line with no voltage regulation and power factor being 0.85. Figure 6 illustrates the relationship between forward capacity boundary and lower voltage boundary with different feeder lengths.

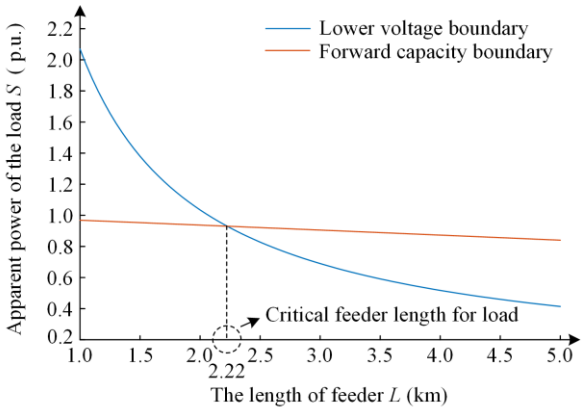

Fig. 6. The relationship between forward capacity boundary and lower voltage boundary with different feeder lengths.

Analysis of Fig. 6 reveals that as the feeder length increases, both the forward capacity boundary and the

lower voltage boundary exhibit a declining trend. The feeder length where these two boundaries intersect corresponds to the CFL for load, determined to be 2.22 km. The calculation of CFL for DG follows a similar procedure, which is not reiterated here.

B. Reference Values Tables of CFL

Following the example of Section IV-A and the calculation conditions of conductor type and its parameters, system operation parameters in Appendix C, Table I and Table II are calculated, which contain the reference values of CFLs for load/DG under typical conductors, PF, and VRMs. VRMs include on-load tap changer (OLTC) and reactive power regulation. Reactive power regulation includes reactive power compensation (RPC) and reactive power absorption (RPA).

TABLE I
REFERENCE VALUES OF CRITICAL FEEDER LENGTH FOR LOAD IN 10 KV DISTRIBUTION SYSTEM DURING NORMAL OPERATION (*N*-0) IN URBAN AND RURAL AREAS

Conductor	PF	Critical feeder length for load (km)						
		No VRMs	U_S = 1.05 p.u.	RPC	U_S = 1.05 p.u. & RPC	U_S = 0.95 p.u.	RPA	U_S = 0.95 p.u. & RPA
YJV22-3×240	0.85	8.64	14.78	9.04	15.42	2.47	8.41	2.40
	0.90	8.94	15.27	9.52	16.21	2.56	8.56	2.45
	0.95	9.50	16.17	10.40	17.60	2.74	8.90	2.55
LGJ-185	0.85	2.22	3.78	2.38	4.02	0.64	2.11	0.61
	0.90	2.38	4.02	2.59	4.35	0.69	2.22	0.64
	0.95	2.64	4.44	2.96	4.92	0.77	2.41	0.70
LGJ-120	0.85	2.37	4.05	2.51	4.28	0.68	2.28	0.65
	0.90	2.47	4.21	2.68	4.54	0.71	2.34	0.67
	0.95	2.66	4.51	2.97	5.00	0.77	2.45	0.70

TABLE II
REFERENCE VALUES OF CRITICAL FEEDER LENGTH FOR DG IN 10KV DISTRIBUTION SYSTEM DURING NORMAL OPERATION (*N*-0) IN URBAN AND RURAL AREAS

Conductor	PF	Critical feeder length for DG (km)						
		No VRMs	U_S = 1.05 p.u.	RPC	U_S = 1.05 p.u. & RPC	U_S = 0.95 p.u.	RPA	U_S = 0.95 p.u. & RPA
YJV22-3×240	0.85	8.70	2.48	8.45	2.41	14.95	9.09	15.66
	0.90	9.05	2.57	8.65	2.47	15.59	9.65	16.70
	0.95	9.73	2.75	9.07	2.58	16.85	10.69	18.66
LGJ-185	0.85	2.29	0.65	2.16	0.62	3.97	2.45	4.28
	0.90	2.48	0.70	2.30	0.65	4.34	2.73	4.81
	0.95	2.85	0.79	2.56	0.72	5.06	3.26	5.94
LGJ-120	0.85	2.39	0.68	2.30	0.68	4.12	2.54	4.39
	0.90	2.52	0.72	2.37	0.72	4.34	2.73	4.75
	0.95	2.74	0.78	2.51	0.78	4.77	3.09	5.45

V. APPLICATION IN NETWORK RECONFIGURATION

Network reconfiguration involves vital process of isolating faults and establishing an optimal power supply restoration scheme through switch operations when a fault arises in the distribution systems [31]. Given the stringent demands on computation time for real-time online application of network reconfiguration, this problem is chosen to validate the proposed method. To ensure seamless implementation, the network reconfiguration model from a source [31] is employed. This model is solved using the fundamental loop encoding approach [32] in conjunction with the classical discrete binary particle swarm algorithm [33].

A. Case Overview

The modified IEEE 33-bus system is utilized for this study, and its configuration is depicted in Fig. 7. The system employs LGJ-185 conductor with a resistance of 0.18 Ω per kilometer and a reactance of 0.37 Ω per kilometer, while having a total capacity of 8.920 MVA. The branch length is 0.05 km and the main trunk length is 0.85 km. The system consists of 32 sectional switches (S1-S32) and 5 tie switches (S33-S37). Load coefficient can be found in Appendix D, Table D1. In the objective function, the weight coefficients a, b, and c are set as 0.6, 0.3, and 0.1, respectively. The operating range of voltage offset is ±7 %, the base capacity is 8.920 MVA, and the load data are provided in Appendix D, Table D2.

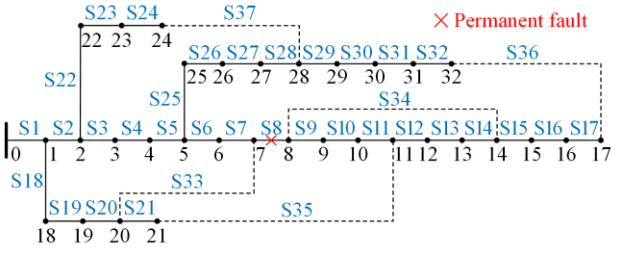

Fig. 7. The modified IEEE 33-bus distribution system for network reconfiguration.

B. Simplification

Referencing Table I, the CFL of LGJ-185 conductor for load is determined to be 2.22 km, assuming a power factor of and No VRMs.

In the event of a permanent fault and the subsequent isolation of the S8 branch, the load node furthest from the slack bus during the network reconfiguration process is identified as node 8. The set of disconnected switches at this point is [S2 S8 S21 S28 S34], and the distance from node 8 to the slack bus measures 1.40 km. This distance is found to be less than the CFL for load, which is 2.22 km, thereby satisfying condition 1. Since the traditional distribution network under consideration does not involve DG, only condition 1 of the simplification criteria needs to be met. As a result, adopting the DC power flow model for simplification is appropriate in this scenario. A comparison between the model before and after this simplification is provided in Table III.

TABLE III
NETWORK RECONFIGURATION MODEL BEFORE AND AFTER SIMPLIFICATION

Items	Modified [31] model (Before simplification)	Model in this paper (After simplification)
Objective function	$\min f = a\dfrac{\sum_{i=1}^{M} P(i)_{\text{cut}}}{\sum_{i_0=1}^{M_0} P(i_0)_{\text{cut}}} + b\dfrac{\sum_{j=1}^{M} L(j)_{\text{cut}}}{\sum_{j_0=1}^{M_0} L(j_0)_{\text{cut}}} + c\dfrac{\sum_{k=1}^{N} K(k)}{N}$	
Equality constraint	$\begin{cases} P_i = U_i \sum_{j=1}^{n} U_j (G_{ij}\cos\theta_{ij} + B_{ij}\sin\theta_{ij}) \\ Q_i = U_i \sum_{j=1}^{n} U_j (G_{ij}\sin\theta_{ij} - B_{ij}\cos\theta_{ij}) \end{cases}$	$P_i = \sum_{j=1}^{n}\left[B_{ij}(\theta_i - \theta_j)\right]$
Inequality constraint	$S_{ij} \leqslant S_{ij,\max}$ $U_{i,\min} \leqslant U_i \leqslant U_{i,\max}$	$S_{ij} \leqslant S_{ij,\max}$
Topological constraint	$g_k \in G_R$	

Table III shows the network reconfiguration model before and after simplification. Firstly, the objective function is to minimize the weighted sum of three components: the total active power of the outage load, the importance of the outage load, and the number of switching actions [31]. Moreover, there exists an equality constraint associated with the power flow equation. The modified [31] model is based on an AC power flow model, which can be transformed into a simplified DC power flow model using the proposed acceleration method in this paper. Furthermore, there are inequality constraints in the form of capacity constraints and voltage constraints within the modified [31] model. With the proposed acceleration method, the optimization model can be streamlined by disregarding the voltage constraints and focusing solely on the capacity constraints. Finally, the topological constraint and load shedding strategy are the same before and after simplification.

Load shedding strategy is introduced as follows. In cases where the branch capacity or node voltage exceeds predefined limits, load shedding becomes necessary following specific guidelines. The strategy for load shedding is structured as follows: 1) Only loads within the non-fault loss power area are eligible for shedding; loads on the normal lines must not be shed; 2) Loads are divided into three categories: the first-level load, second-level load and third-level load; 3) Load curtailment begins with the third-level loads and proceeds in ascending order of load magnitude. If, after each round of curtailment, the voltage and capacity constraints are no longer breached, the load shedding process concludes. However, if the voltage or capacity limits are still violated post-curtailment, further measures target loads with greater magnitude and higher importance coefficients.

C. Verification

1) Verification by Network Reconfiguration Results

The simplified model, as well as the modified model in [31], are independently solved. A comprehensive comparison of the resultant solutions along with the computation times is presented in Table IV.

Table IV clearly demonstrates that the model can be simplified based on the proposed method. The network reconfiguration results after simplification align perfectly with the method presented in [31]. Notably, this simplification yields a remarkable reduction in computation time by 19.923%, showcasing a highly significant acceleration effect.

TABLE IV
COMPARISON OF NETWORK RECONFIGURATION RESULTS BEFORE AND AFTER SIMPLIFICATION

Items	Modified [31] model (Before simplification)	Model in this paper (After simplification)
Disconnected switch set	[S8 S33 S34 S36 S37]	[S8 S33 S34 S36 S37]
Number of switch operations	1	1
Load nodes for outage	8, 9, 14, 15	8, 9, 14, 15
Total power of the outage load (kW)	520	520
Restored load (%)	87.348	87.348
Objective function value	0.176	0.176
The minimum voltage (p.u.)	0.993	0.993
The maximum voltage (p.u.)	1	1
The computation time (t/s)	46.389	37.147

2) Verification by Security Boundary Visualization

Further verification is conducted through security boundary visualization. When meeting Condition 1, the lower voltage constraints can be neglected, and the DC power flow model is adopted for model simplification. For the IEEE 33-bus system illustrated in Fig. 7, observational two-dimensional security boundary view is obtained for node 12 and node 29, as depicted in Fig. 8.

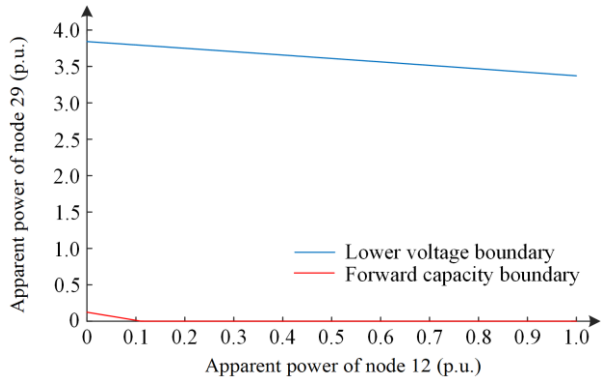

Fig. 8. Two-dimensional view of the security boundary for the IEEE 33-bus system.

Figure 8 clearly shows that the forward capacity boundary is contained within the lower voltage boundary, indicating that the forward capacity constraints are more stringent than the lower voltage constraints. As a result, the lower voltage constraints can be disregarded.

However, it is important to recognize that the method discussed in this paper may not be universally applicable to all distribution systems in network reconfiguration problems. Specifically, in systems with long feeders and substantial loads, the proposed simplification method may not fully align with voltage constraint requirements. For a more detailed discussion of such cases, please refer to the example presented in Appendix E.

VI. APPLICATION IN REACTIVE POWER OPTIMIZATION

Reactive power optimization is essential for efficiently distributing reactive power by adjusting various devices to minimize network losses or achieve other objectives [34]. Given its critical role in distribution system optimization, it serves as an appropriate choice for validating the proposed method. In this study, the reactive power optimization model is adapted from [35]. The solution method utilizes the classical particle swarm optimization algorithm for implementation.

A. Case Overview

Figure 9 shows the modified IEEE 33-bus system for reactive power optimization. The system employs LGJ-185 conductor, and it's worth noting that the branch length is 0.10 km, with the main trunk extending to 1.70 km.

The system incorporates a set of voltage regulation and reactive power equipment, including two DGs capable of supplying reactive power to the distribution system. Additionally, there are two sets of parallel compensation capacitors with capacities of 0.15 Mvar×4 and 0.15 Mvar×7, respectively. Both DGs play a role in voltage regulation, with their active output set at 1 MW, and the reactive output within the range of –0.1 Mvar to 0.5 Mvar. The operating range for voltage offset is set at ±7%. The unit value reference capacity is 8.920 MVA, and the load data are shown in Appendix F, Table F1.

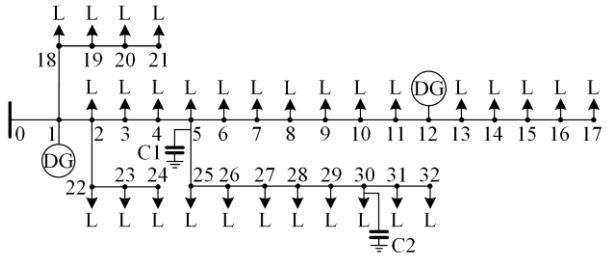

Fig. 9. The modified IEEE 33-bus distribution system for reactive power optimization.

B. Simplification

Look up the Table I, the CFL of LGJ-185 conductor for load is determined to be 2.22 km, assuming a 0.85 power factor and No VRMs. Look up the Table II, the CFL of LGJ-185 conductor for DG is determined to be 2.29 km, assuming a 0.85 power factor and No VRMs.

The terminal load node, in relation to the slack bus, is identified as node 17, with a distance of 1.70 km, falling

within the CFL for load (2.22 km), thereby satisfying condition 1. Additionally, the terminal DG node to the slack bus is node 12, situated at a distance of 1.20 km, which is less than the CFL for DG (2.29 km), satisfying condition 2. Both conditions are met, making it possible to simplify the case in line with the simplification criteria.

Whereas it is theoretically possible to simplify the case by adopting the DC power flow model or by disregarding the voltage constraints, it's important to note that the reactive power optimization problem requires the calculation of both voltage and network loss. As such, directly adopting the DC power flow model for simplification is not feasible in this context. However, the model can still be simplified by disregarding the voltage constraints, which is a viable method.

A comparison between the model before and after this simplification is shown in Table V.

TABLE V
REACTIVE POWER OPTIMIZATION MODEL OF ACTIVE DISTRIBUTION NETWORK BEFORE AND AFTER SIMPLIFICATION

Items	Modified [35] model (Before simplification)	Model in this paper (After simplification)
Objective function	$F=\min\left\{P_{\text{loss}}+\lambda\sum_{i=1}^{n}\left(\frac{\Delta U_i}{U_{i,\max}-U_{i,\min}}\right)^2\right\}$ $P_{\text{loss}}=\sum_{k=1}^{m}G_{k,ij}(U_i^2+U_j^2-2U_iU_j\cos\theta_{ij})$ $\Delta U_i=\begin{cases}U_{i,\min}-U_i(U_i<U_{i,\min})\\0(U_{i,\min}\leqslant U_i\leqslant U_{i,\max})\\U_i-U_{i,\max}(U_i>U_{i,\max})\end{cases}$	$P_{\text{loss}}=\sum_{k=1}^{m}G_{k,ij}(U_i^2+U_j^2-2U_iU_j\cos\theta_{ij})$
Equality constraint	$\begin{cases}P_i=U_i\sum_{j=1}^{n}U_j(G_{ij}\cos\theta_{ij}+B_{ij}\sin\theta_{ij})\\Q_i=U_i\sum_{j=1}^{n}U_j(G_{ij}\sin\theta_{ij}-B_{ij}\cos\theta_{ij})\end{cases}$	
Inequality constraint	$Q_{\text{DG},x,\min}\leqslant Q_{\text{DG},x}\leqslant Q_{\text{DG},x,\max}$ $Q_{\text{C},y,\min}\leqslant Q_{\text{C},y}\leqslant Q_{\text{C},y,\max}$ $S_{ij}\leqslant S_{ij,\max}$ $U_{i,\min}\leqslant U_i\leqslant U_{i,\max}$	$Q_{\text{DG},x,\min}\leqslant Q_{\text{DG},x}\leqslant Q_{\text{DG},x,\max}$ $Q_{\text{C},y,\min}\leqslant Q_{\text{C},y}\leqslant Q_{\text{C},y,\max}$ $S_{ij}\leqslant S_{ij,\max}$

Table V shows the reactive power optimization model of active distribution network before and after simplification. Regarding the objective function, the penalty function of active power loss and node voltage over-limit is taken as the comprehensive objective function in the modified [35] model. In this paper, only active power loss is taken as the objective function. In terms of inequality constraints, the modified [35] model includes both capacity constraints and voltage constraints. According to the proposed acceleration method in this paper, the optimization model can be streamlined by disregarding the voltage constraints and focusing solely on the capacity constraints.

C. Verification

The simplification of the case involves disregarding the voltage constraints. The simplified model, as well as the modified model is presented in [35], are independently solved. Then, a thorough comparison is provided in Table VI.

TABLE VI
COMPARISON OF REACTIVE POWER OPTIMIZATION RESULTS BEFORE AND AFTER SIMPLIFICATION

Items	Modified [35] model (Before simplification)	Model in this paper (After simplification)
Capacitor $Q_{\text{C},1}$ capacity/ (kvar)	600	600
Capacitor $Q_{\text{C},2}$ capacity (kvar)	300	300
Reactive power output of DG1 $Q_{\text{DG},1}$ (kvar)	483.39	476.57
Reactive power output of DG2 $Q_{\text{DG},2}$ (kvar)	351.08	354.50
The minimum voltage (p.u.)	0.998	0.998
The maximum voltage (p.u.)	1	1
The objective value (Active power loss) (kW)	2.896	2.896
The computation time (t/s)	2.459	2.134

Table VI clearly indicates that the simplification made in this paper has led to the exclusion of voltage constraints from the original model. Despite this adjustment, the achieved optimization outcomes for reactive power remain closely in line with the method outlined in [35], and the objective value is the same as that of the method in [35]. Furthermore, the calculation time has been reduced by 13.217%, illustrating a noticeable acceleration effect.

The proposed method in this paper not only directly simplifies and accelerates the optimization model but also can be integrated with existing simplification methods, such as convex relaxation method [17], to further improve the solution speed. The comparative results of combining convex relaxation method with the proposed method are presented in Table VII.

TABLE VII
COMPARISON OF REACTIVE POWER OPTIMIZATION RESULTS BEFORE AND AFTER COMBINING THE PROPOSED METHOD IN CONVEX RELAXATION METHOD

Items	Convex relaxation method [17]	Convex relaxation method [17] + the proposed method
Capacitor $Q_{C,1}$ capacity (kvar)	450	450
Capacitor $Q_{C,2}$ capacity (kvar)	300	300
Reactive power output of DG1 $Q_{DG,1}$ (kvar)	499.99	499.98
Reactive power output of DG2 $Q_{DG,2}$ (kvar)	394.63	394.68
The minimum voltage (p.u.)	0.998	0.998
The maximum voltage (p.u.)	1	1
The objective value (Active power loss) (kW)	2.892	2.892
The computation time (t/s)	0.771	0.729

As seen in Table VII, the combination of convex relaxation method with the proposed method results in a 5.45% reduction in computation time, while maintaining nearly unchanged outcomes. This further validates the effectiveness of the method proposed in this paper.

However, it's important to acknowledge that not all reactive power optimization scenarios can be effectively addressed using the method discussed in this paper. Specifically, there are certain distributed systems characterized by long feeders and heavy loads where the proposed method for simplification no longer adheres to the voltage constraint requirements. A detailed illustration of such scenario can be found in Appendix G.

VII. CONCLUSION

Real-world distribution systems are typically large in scale, imposing significant requirements on the computation speed for their online applications. To address this challenge, this paper introduces a general simplification and acceleration method for optimization problems in distribution systems that integrate power flow equations or voltage constraints based on DSSR theory. The primary conclusions of this paper can be summarized as follows:

1) CFLs for load and DG form the basis of the simplification criteria. The criteria are tools for determining the feasibility of simplification by analyzing the relationship between the distance from the end load/DG node to the slack bus and the respective CFL.

2) A significant portion of urban distribution systems align with the simplification criteria. For systems meeting these criteria, the optimization model can leverage either the DC power flow model or discard the voltage constraints, resulting in effective simplification and significant acceleration.

3) The proposed method is validated through its application to network reconfiguration and reactive power optimization problems. Remarkable reductions in computation time, 19.9% and 13.2% respectively, are achieved for the modified IEEE 33-bus system while maintaining a high level of accuracy.

This method is widely applicable to optimization problems integrating power flow equations or voltage constraints in both active and traditional distribution networks across diverse settings. The proposed method can not only be used independently but also be combined with other acceleration methods, such as convex relaxation method. Future research will focus on continued validation and refinement of the method in various scenarios, as well as further exploration of the theoretical foundations of the simplification criteria.

APPENDIX A

A. Terminology

The key terminology is provided in Table A1.

TABLE A1
LIST OF IMPORTANT TERMINOLOGY

Terminology	Definition
Security boundary	The boundary of the DSSR, composed of operating points linked to the smallest possible load increase that could render the system insecure [26].
Capacity boundary	The security boundary when the voltage constraints are disregarded and only limited by the capacity constraints [22].
Forward capacity boundary	The capacity boundary when the power flow reaches the forward boundary in which an increase in load or a decrease in DG output typically results in a violation of the forward capacity constraints.

CONTINUED

Terminology	Definition
Reverse capacity boundary	The capacity boundary when the power flow reaches the reverse boundary in which a decrease in load or an increase in DG output typically results in a violation of the reverse capacity constraints.
Voltage boundary	The security boundary when the capacity constraints are disregarded and only limited by the voltage constraints [22].
Lower voltage boundary	The voltage boundary when the voltage magnitude reaches the lower voltage boundary in which an increase in load or a decrease in DG output typically results in a violation of the lower voltage constraints.
Upper voltage boundary	The voltage boundary when the voltage magnitude reaches the upper voltage boundary in which a decrease in load or an increase in DG output typically results in a violation of the upper voltage constraints.
Critical feeder length	The critical length of conversion between capacity constraints and voltage constraints in traditional distribution network [22].
Critical feeder length for load	The critical length of the distance from the end load node to the slack bus in the distribution system, which is used to separate the forward capacity constraints from the lower voltage constraints.

APPENDIX B

B. Calculation Method of the Total Load/DG per Unit Value Corresponding to the Capacity/Voltage Boundary Point

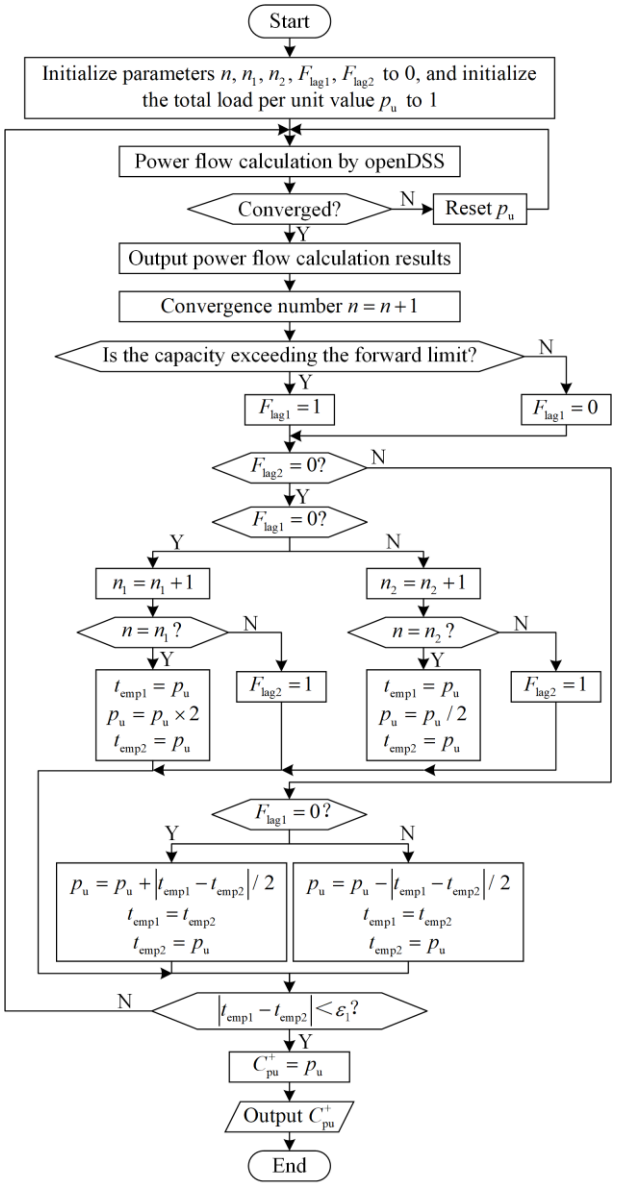

Fig. B1. Calculation process of the total load per unit value C_{pu}^{+} corresponding to the forward capacity boundary point.

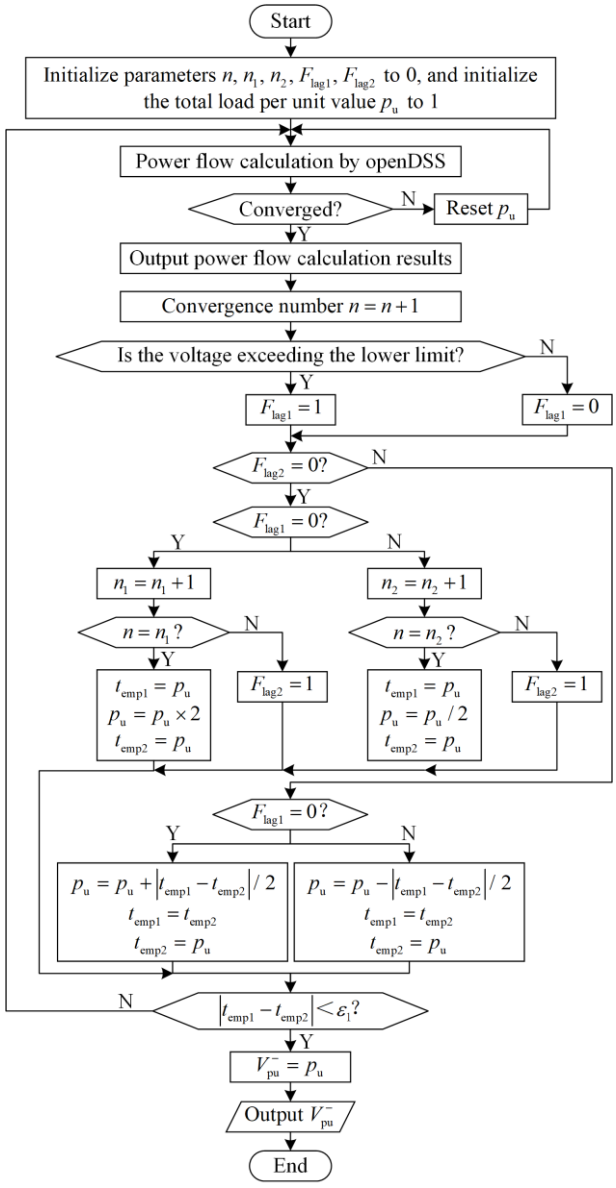

Fig. B2. Calculation process of the total load per unit value V_{pu}^{-} corresponding to the lower voltage boundary point.

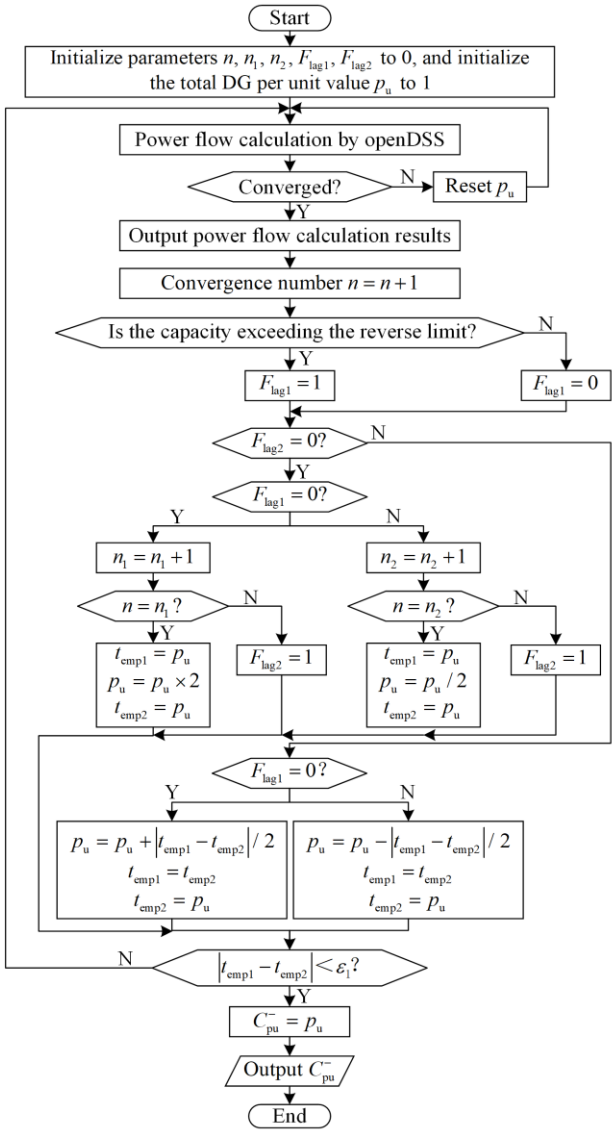

Fig. B3. Calculation process of the total DG per unit value C_{pu}^- corresponding to the reverse capacity boundary point.

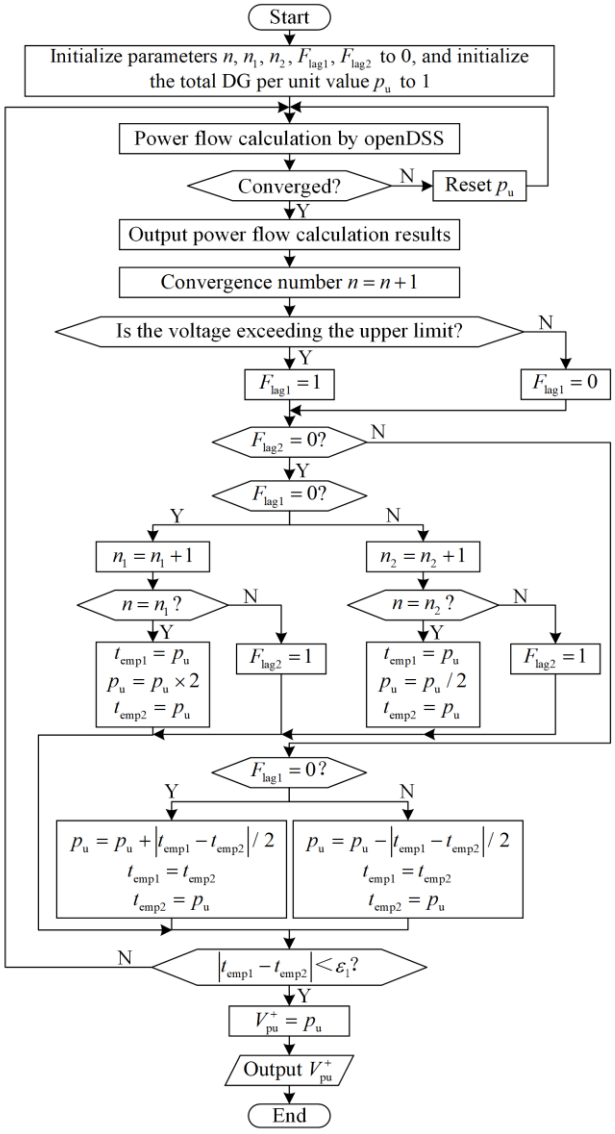

Fig. B4. Calculation process of the total DG per unit value V_{pu}^+ corresponding to the upper voltage boundary point.

APPENDIX C

C. Calculation Conditions of Critical Feeder Length Table for Load/DG

The calculation conditions include conductor type and its parameters, and system operation parameters. The conductors selected for calculating the CFL for load/DG are detailed in Table C1, while the system operation parameters are outlined in Table C2.

TABLE C1
CONDUCTORS TYPE AND PARAMETERS

Type	Area	Reactance (Ω/km)	Resistance (Ω/km)	Current-carrying capability (A)
YJV22-3×240	urban area	0.09	0.08	404
LGJ-185	town area	0.37	0.18	515
LGJ-120	rural area	0.38	0.29	380

TABLE C2
SYSTEM OPERATION PARAMETERS

PF	VRMs	Slack bus voltage U_S before voltage regulation (p.u.)	Slack bus voltage U_S after voltage regulation (p.u.)	Load/DG node voltage $U_{L,min}$ (p.u.)	Load/DG node voltage $U_{L,max}$ (p.u.)
0.85 0.90 0.95	OLTC RPC RPA	1.00	0.95/1.05	0.93	1.07

Note: The reference voltage is $U_N = 10\,\text{kV}$.

APPENDIX D

D. Data of Network Reconfiguration Problem

1) Load Coefficient

The load classification and coefficient of IEEE 33-bus system are shown in Table D1.

TABLE D1
LOAD COEFFICIENT OF IEEE 33-BUS SYSTEM

Load classification	Coefficient	Node
First-level load	10	1、10、11、17、27
Second-level load	5	4、6、7、18、19、21、23、26、32
Third-level load	1	2、3、5、8、9、12-16、20、22、24、25、28-31

2) Load Data

TABLE D2
LOAD DATA OF IEEE 33-BUS SYSTEM FOR RECONFIGURATION

Node	Load (kW+kvar)	Power factor
1	120+j60	0.89
2	90+j40	0.91
3	100+j60	0.86
4	60+j30	0.89
5	60+j20	0.95
6	200+j100	0.89
7	200+j100	0.89
8	100+j60	0.86
9	60+j20	0.95
10	100+j60	0.86
11	600+j350	0.86
12	1200+j600	0.89
13	1000+j600	0.86
14	60+j10	0.99
15	300+j100	0.95
16	600+j200	0.95
17	90+j40	0.91
18	900+j400	0.91
19	90+j40	0.91
20	900+j400	0.91
21	90+j40	0.91
22	90+j50	0.87
23	420+j200	0.90
24	100+j60	0.86
25	60+j25	0.92
26	60+j25	0.92
27	60+j20	0.95
28	120+j70	0.86
29	1000+j600	0.86
30	150+j70	0.91
31	210+j100	0.90
32	100+j60	0.86

APPENDIX E

E. Illustration of a Network Reconfiguration Problem Incompatible with the Proposed Method

To illustrate a scenario where the voltage drops below the lower limit during the network reconfiguration of the distribution system, modifications are made to the branch length, extending it to 0.80 km, while the main trunk is increased to 13.60 km. These changes are applied to the modified IEEE 33-bus distribution system depicted in Fig. 7. Furthermore, adjustments are made to certain loads, as detailed in Table E1.

TABLE E1
LOAD DATA OF NETWORK RECONFIGURATION PROBLEM INCOMPATIBLE WITH THE PROPOSED METHOD

Node	Load (kW+kvar)	Power factor
1	1200+j600	0.89
2	90+j40	0.91
3	100+j60	0.86
4	60+j30	0.89
5	60+j20	0.95
6	200+j100	0.89
7	200+j100	0.89
8	500+j300	0.86
9	300+j100	0.95
10	100+j60	0.86
11	60+j35	0.86
12	600+j300	0.89
13	500+j300	0.86
14	60+j10	0.99
15	120+j40	0.95
16	300+j100	0.95
17	90+j40	0.91
18	450+j200	0.91
19	90+j40	0.91
20	90+j40	0.91
21	90+j40	0.91
22	90+j50	0.87
23	420+j200	0.90
24	100+j60	0.86
25	60+j25	0.92
26	60+j25	0.92
27	60+j20	0.95
28	120+j70	0.86
29	100+j60	0.86
30	150+j70	0.91
31	210+j100	0.90
32	100+j60	0.86

The end load node, situated at a distance of 10.40 km from the slack bus, is designated as node 32. This distance exceeds the CFL for load (2.22 km), thereby not meeting condition 1 when the permanent fault of the S8 branch occurs and is isolated. In this scenario, the AC

power flow model is utilized, and the voltage constraints are considered in alignment with the simplification criteria. Then, Table E2 displays the comparison results.

TABLE E2
COMPARISON OF NETWORK RECONFIGURATION RESULTS

Items	Modified [31] model (Before simplification)	Model in this paper (After simplification)
Disconnected switch set	[S8 S33 S34 S36 S37]	[S8 S33 S34 S36 S37]
Number of switch operations	1	1
Load nodes for outage	9、14、15	/
Total power of the outage load (kW)	480	0
Restored load (%)	81.749	100
Objective function value	0.185	0.003
The minimum voltage (p.u.)	0.931	0.921
The maximum voltage (p.u.)	1	1

Table E2 clearly demonstrates that the simplified model exhibits significant discrepancies in results when compared to the original model. Furthermore, the minimum voltage is 0.921 p.u. after simplification, which falls outside the permissible voltage constraint of ±7%. This underscores the necessity of employing the AC power flow model for distribution system examples and considering the voltage constraints.

APPENDIX F

F. Data of Reactive Power Optimization Problem

TABLE F1
LOAD DATA OF IEEE 33-BUS SYSTEM FOR REACTIVE POWER OPTIMIZATION

Node	Load (kW+kvar)	Power factor
1	120+j60	0.89
2	90+j40	0.91
3	100+j60	0.86
4	60+j30	0.89
5	60+j20	0.95
6	200+j100	0.89
7	200+j100	0.89
8	100+j60	0.86
9	60+j20	0.95
10	100+j60	0.86
11	60+j35	0.86
12	120+j60	0.89
13	100+j60	0.86
14	60+j10	0.99
15	60+j20	0.95
16	60+j20	0.95
17	90+j40	0.91
18	90+j40	0.91
19	90+j40	0.91
20	90+j40	0.91
21	90+j40	0.91
22	90+j50	0.87
23	420+j200	0.90
24	100+j60	0.86
25	60+j25	0.92
26	60+j25	0.92
27	60+j20	0.95
28	120+j70	0.86
29	100+j60	0.86
30	150+j70	0.91
31	210+j100	0.90
32	100+j60	0.86

APPENDIX G

G. Illustration of a Reactive Power Optimization Problem Incompatible with the Proposed Method

To illustrate a scenario where the voltage drops below the lower limit during the reactive power optimization of the active distribution network, modifications are made to the branch length, extending it to 1.00 km, while the main trunk is increased to 17.00 km. The operating range for voltage offset is set at ±5%. These changes are applied to the modified IEEE 33-bus distribution system depicted in Fig. 9. Furthermore, adjustments are made to certain loads, as detailed in Table G1.

TABLE G1
LOAD DATA OF THE REACTIVE POWER OPTIMIZATION PROBLEM INCOMPATIBLE WITH THE PROPOSED METHOD

Node	Load (kW+kvar)	Power factor
1	120+j60	0.89
2	90+j40	0.91
3	100+j60	0.86
4	60+j30	0.89
5	60+j20	0.95
6	200+j100	0.89
7	200+j100	0.89
8	120+j60	0.89
9	60+j20	0.95
10	100+j60	0.86
11	60+j35	0.86
12	1200+j600	0.89
13	100+j60	0.86
14	60+j10	0.99
15	60+j20	0.95
16	60+j20	0.95
17	90+j40	0.91
18	90+j40	0.91
19	90+j40	0.91
20	90+j40	0.91
21	90+j40	0.91
22	90+j50	0.87
23	420+j200	0.90
24	100+j60	0.86
25	60+j25	0.92
26	60+j25	0.92
27	60+j20	0.95
28	120+j70	0.86
29	100+j60	0.86
30	150+j70	0.91
31	210+j100	0.90
32	100+j60	0.86

The end load node connected to the slack bus is identified as node 17, with a distance of 17.00 km, which exceeds the CFL for load (2.22 km), thereby not meeting condition 1. Additionally, the end DG node to the slack bus is node 12, situated 12.00 km away, which also exceeds the CFL for DG (2.29 km), thus not meeting condition 2. In this scenario, the AC power flow model is utilized, and the voltage constraints are considered in alignment with the simplification criteria. The comparison results are presented in Table G2.

TABLE G2
COMPARISON OF THE REACTIVE POWER OPTIMIZATION RESULTS

Items	Modified [35] model (Before simplification)	Model in this paper (After simplification)
Capacitor $Q_{C,1}$ capacity (kvar)	600	600
Capacitor $Q_{C,2}$ capacity (kvar)	750	600
Reactive power output of DG1 $Q_{DG,1}$ (kvar)	475.99	369.90
Reactive power output of DG2 $Q_{DG,2}$ (kvar)	498.37	485.41
The minimum voltage (p.u.)	0.951	0.947
The maximum voltage (p.u.)	1	1
The objective value (Active power loss) (kW)	87.810	87.694

Table G2 clearly demonstrates that the simplified model shows significant discrepancies compared to the original model. Furthermore, the minimum voltage after simplification is 0.947 p.u., which falls outside the permissible voltage constraint of ±5%. This highlights the importance of employing the AC power flow model for distribution system cases and considering voltage constraints.

ACKNOWLEDGMENT

Not applicable.

AUTHORS' CONTRIBUTIONS

Jun Xiao: resources, supervision, conceptualization, methodology, the construction of the paper framework. Yupeng Zhou: methodology, software and simulations, data analysis, validation, full-text writing. Buxin She: methodology, polishing. Zhenyu Bao: methodology. All authors read and approved the final manuscript.

FUNDING

This work is supported by the National Natural Science Foundation of China (No. 52177105).

AVAILABILITY OF DATA AND MATERIALS

Not applicable.

DECLARATIONS

Competing interests: The authors declare that they have no known competing financial interests or personal relationships that could have appeared to influence the work reported in this article.

AUTHORS' INFORMATION

Jun Xiao received the B.S., M.S. and Ph.D. degrees in electrical engineering from Tianjin University, Tianjin, China. He was a visiting scholar in department of Electrical Engineering and Computer Science, University of Tennessee, Knoxville, USA. He is now a professor with the School of Electrical and Information Engineering, Tianjin University. His research interests include distribution system planning and security, network theory.

Yupeng Zhou was born in Tianjin, China in 2000. He received the B.S. degree from the Dalian Maritime University in 2022. He received the M.S. degree from the Tianjin University in 2024. Currently, he is a Ph.D. student in Tianjin University. His research interests include distribution system planning and security.

Buxin She is a Ph.D. student in the Department of Electrical Engineering and Computer Science, University of Tennessee, Knoxville, USA. He received his B.S. and M.S. degrees both from Tianjin University, Tianjin, China in 2017 and 2019, respectively. He was an outstanding reviewer of MPCE and IEEE OAJPE. He is a student guest editor of IET-RPG. His research interests include microgrid operation and control, machine learning in power systems, distribution system operation and plan, and power grid resilience.

Zhenyu Bao received the B.S. and M.S. degrees both from Tianjin University, Tianjin, China in 2019 and 2022, respectively.

REFERENCES

[1] G. Dileep, "A survey on smart grid technologies and applications," *Renewable Energy*, vol. 146, pp. 2589-2625, Feb. 2020.

[2] A. M. Shaheen, R. A. El-Sehiemy, and H. M. Hasanien *et al*., "An improved heap optimization algorithm for efficient energy management based optimal power flow model," *Energy*, vol. 250, no. 123795, Jul. 2022.

[3] H. Yuan, F. Li, and Y. Wei *et al*., "Novel linearized power flow and linearized OPF models for active distribution networks with application in distribution LMP," *IEEE Transactions on Smart Grid*, vol. 9, no. 1, pp. 438-448, Jan. 2018.

[4] Z. Yang, H. Zhong, and A. Bose *et al*., "A linearized OPF model with reactive power and voltage magnitude: a pathway to improve the MW-Only DC OPF," *IEEE Transactions on Power Systems*, vol. 33, no. 2, pp. 1734-1745, Mar. 2018.

[5] J. Zhang, M. Cui, and B. Li *et al*., "Fast solving method based on linearized equations of branch power flow for coordinated charging of EVs (EVCC)," *IEEE Transactions on Vehicular Technology*, vol. 68, no. 5, pp. 4404-4418, May 2019.

[6] D. Jin, H. D. Chiang, and P. Li *et al*., "Two-timescale multi-objective coordinated volt/var optimization for active distribution networks," *IEEE Transactions on Power Systems*, vol. 34, no. 6, pp. 4418-4428, Nov. 2019.

[7] H. D. M. Braz and B. A. de Souza, "Distribution network reconfiguration using genetic algorithms with sequential encoding: subtractive and additive approaches," *IEEE Transactions on Power Systems*, vol. 26, no. 2, pp. 582-593, May 2011.

[8] J. Liu, H. Cheng, and P. Zeng *et al*., "Rapid assessment of maximum distributed generation output based on security distance for interconnected distribution networks," *International Journal of Electrical Power & Energy Systems*, vol. 101, pp. 13-24, Oct. 2018.

[9] J. Xiao, F. Li, and W. Gu *et al*., "Total supply capability and its extended indices for distribution systems: definition, model calculation and applications," *IET Generation, Transmission & Distribution*, vol. 5, no. 8, pp. 869-876, Aug. 2011.

[10] B. She, F. Li, and H. Cui *et al*., "Decentralized and coordinated Vf control for islanded microgrids considering DER inadequacy and demand control", *IEEE Transactions on Energy Conversion*, vol. 38, no. 3, pp. 1868-1880, Sep. 2023.

[11] F. Zhang and C. Cheng, "A modified Newton method for radial distribution system power flow analysis," *IEEE Transactions on Power Systems*, vol. 12, no. 1, pp. 389-397, Feb. 1997.

[12] A. Suchite Remolino, H. F. Ruiz Paredes, and V. Torres García *et al*., "A new approach for PV nodes using an efficient backward/forward sweep power flow technique," *IEEE Latin America Transactions*, vol. 18, no. 6, pp. 992-999, Jun. 2020.

[13] T. Chen, M. Chen, and K. J. Hwang *et al*., "Distribution system power flow analysis-a rigid approach," *IEEE Transactions on Power Delivery*, vol. 6, no. 3, pp. 1146-1152, Jul. 1991.

[14] W. Wu and B. Zhang, "A three-phase power flow algorithm for distribution system power flow based on loop-analysis method," *International Journal of Electrical Power & Energy Systems*, vol. 30, no. 1, pp. 8-15, Jan. 2008.

[15] Z. Li, J. Yu, and Q. Wu *et al*., "Approximate linear power flow using logarithmic transform of voltage magnitudes with reactive power and transmission loss consideration," *IEEE Transactions on Power Systems*, vol. 33, no. 4, pp. 4593-4603, Jul. 2018.

[16] T. Yang, Y. Guo, and L. Deng *et al*., "A linear branch flow model for radial distribution networks and its application to reactive power optimization and network reconfiguration," *IEEE Transactions on Smart Grid*, vol. 12, no. 3, pp. 2027-2036, May 2021.

[17] M. Farivar and S. H. Low, "Branch flow model: relaxations and convexification—part I," *IEEE Transactions on Power Systems*, vol. 28, no. 3, pp. 2554-2564, Aug. 2013.

[18] M. Farivar and S. H. Low, "Branch flow model: relaxations and convexification—part II," *IEEE Transactions on Power Systems*, vol. 28, no. 3, pp. 2565-2572, Aug. 2013.

[19] C. Li, S. Miao, and Y. Li *et al*., "Coordinating dynamic network reconfiguration with ANM in active distribution network optimisation considering system structure security evaluation," *IET Generation, Transmission & Distribution*, vol. 13, no. 19, pp. 4355-4363, Oct. 2019.

[20] B. She, F. Li, and H. Cui *et al*., "Virtual inertia Scheduling (VIS) for real-time economic dispatch of IBR-penetrated power systems," *IEEE Transactions on Sustainable Energy*, vol. 15, no. 2, pp. 938-951, Apr. 2024.

[21] J. Yang, N. Zhang, and C. Kang *et al*., "A state-independent linear power flow model with accurate estimation of voltage magnitude," *IEEE Transactions on Power Systems*, vol. 32, no. 5, pp. 3607-3617, Sep. 2017.

[22] J. Xiao, Z. Bao, and C. Song *et al*., "Power flow model selection method of distribution network analysis and optimization," *IEEE PES General Meeting*, Washington, DC, USA, Jul. 2021, pp. 1-5.

[23] J. Xiao, Y. Zhou, and Z. Bao, "Power flow model selection method for modeling distribution system optimization problem," *Automation of Electric Power Systems*, vol. 47, no. 15, pp. 170-178, Apr. 2023. (in Chinese)

[24] G. Zu, J. Xiao, and K. Sun *et al*., "Mathematical base and deduction of security region for distribution systems with DER," *IEEE Transactions on Smart Grid*, vol. 10, no. 3, pp. 2892-2903, May 2019.

[25] J. Xiao, G. Zu, and H. Zhou *et al*., "Total quadrant security region for active distribution network with high penetration of distributed generation," *Journal of Modern Power Systems and Clean Energy*, vol. 9, no. 1, pp. 128-137, Jan. 2021.

[26] J. Xiao, G. Zu, and X. Gong *et al*., "Observation of security region boundary for smart distribution grid," *IEEE Transactions on Smart Grid*, vol. 8, no. 4, pp. 1731-1738, Jul. 2017.

[27] J. Xiao, W. Gu, and C. Wang *et al*., "Distribution system security region: definition, model and security assessment," *IET Generation*, *Transmission & Distribution*, vol. 6, no. 10, pp. 1029-1035, Oct. 2012.

[28] W. Huang, Z. Shuai, and X. Shen *et al*., "Dynamical reconfigurable master-slave control architecture (DRMSCA) for voltage regulation in islanded microgrids," *IEEE Transactions on Power Electronics*, vol. 37, no. 1, pp. 249-263, Jan. 2022.

[29] A. Werth, A. André, and D. Kawamoto *et al*., "Peer-to-peer control system for DC microgrids," *IEEE Transactions on Smart Grid*, vol. 9, no. 4, pp. 3667-3675, Jul. 2018.

[30] R. An, Z. Liu, and J. Liu *et al*., "A comprehensive solution to decentralized coordinative control of distributed generations in islanded microgrid based on dual-frequency-droop," *IEEE Transactions on Power Electronics*, vol. 37, no. 3, pp. 3583-3598, Mar. 2022.

[31] K. Miu, H.D. Chiang, and B. Yuan *et al*., "Fast service restoration for large-scale distribution systems with priority customers and constraints," *IEEE Transactions on Power Systems*, vol. 13, no. 3, pp. 789-795, Aug. 1998.

[32] J. Mendoza, R. López, and D. Morales *et al*., "Minimal loss reconfiguration using genetic algorithms with restricted population and addressed operators: real application," *IEEE Transactions on Smart Grid*, vol. 21, no. 2, pp. 948-954, May 2006.

[33] G. F. Noudjiep Djiepkop and S. Krishnamurthy, "Multi-objective feeder reconfiguration using discrete particle swarm optimization," *Mathematics*, vol. 10, no. 3, Feb. 2022.

[34] C. Dai, W. Chen, and Y. Zhu *et al*., "Seeker optimization algorithm for optimal reactive power dispatch," *IEEE Transactions on Power Systems*, vol. 24, no. 3, pp. 1218-1231, Aug. 2009.

[35] H. Singh, Y. Sawle, and S. Dixit *et al*., "Optimization of reactive power using dragonfly algorithm in DG integrated distribution system," *Electric Power Systems Research*, vol. 220, no. 109351, Jul. 2023.